

# Promoting Photocatalytic Hydrogen Evolution Activity of Graphitic Carbon Nitride with Hole-Transfer Agents

Arindam Indra<sup>+,\*<sup>[a]</sup></sup>, Rodrigo Beltrán-Suito<sup>+,<sup>[b]</sup></sup>, Marco Müller,<sup>[b]</sup> Ramesh P. Sivasankaran,<sup>[c]</sup> Michael Schwarze,<sup>[b]</sup> Amitava Acharjya,<sup>[d]</sup> Bapi Pradhan,<sup>[e]</sup> Johan Hofkens,<sup>[e, f]</sup> Angelika Brückner,<sup>[c]</sup> Arne Thomas,<sup>[d]</sup> Prashanth W. Menezes,<sup>\*<sup>[b]</sup></sup> and Matthias Driess<sup>\*<sup>[b]</sup></sup>

Visible light-driven photocatalytic reduction of protons to H<sub>2</sub> is considered a promising way of solar-to-chemical energy conversion. Effective transfer of the photogenerated electrons and holes to the surface of the photocatalyst by minimizing their recombination is essential for achieving a high photocatalytic activity. In general, a sacrificial electron donor is used as a hole scavenger to remove photogenerated holes from the valence band for the continuation of the photocatalytic hydrogen (H<sub>2</sub>) evolution process. Here, for the first time, the hole-transfer dynamics from Pt-loaded sol-gel-prepared graphitic carbon nitride (Pt-sg-CN) photocatalyst were investigated using different adsorbed hole acceptors along with a sacrificial agent (ascorbic acid). A significant increment (4.84 times) in H<sub>2</sub> production was achieved by employing phenothiazine (PTZ) as the hole acceptor with continuous H<sub>2</sub> production for 3 days. A detailed charge-transfer dynamic of the photocatalytic process in the presence of the hole acceptors was examined by time-resolved photoluminescence and in situ electron paramagnetic resonance studies.

Conversion of photon energy to chemical energy by reducing water into molecular H<sub>2</sub> has the highest prospective of providing clean and sustainable energy to replace fossil fuels.<sup>[1]</sup> An efficient photocatalyst with a suitable band structure can harvest solar light to convert it into chemical energy.<sup>[2]</sup> Among various photocatalysts reported in the literature, the organic semiconductor polymeric graphitic

carbon nitride (*g*-CN) has attained growing interest for the visible-light-induced photocatalytic H<sub>2</sub> evolution reaction (HER) in recent years.<sup>[3]</sup> The appropriate bandgap, conduction band position, high physicochemical stability, and facile large-scale synthesis make *g*-CN proficient for the photocatalytic proton reduction.<sup>[4]</sup> Moreover, the band structure can be engineered by doping with heteroatoms or changing the conjugated structure of the *g*-CN to avail better photocatalytic performance.<sup>[4]</sup> Generally, the photocatalytic activity of *g*-CN largely depends on the choice of the cocatalyst, pH of the reaction medium, and a sacrificial electron donor.<sup>[4]</sup> A noble metal cocatalyst like Pt has shown improvements in the photocatalytic HER rate compared to the bare *g*-CN.<sup>[5]</sup> The use of non-noble cocatalysts with *g*-CN to attain efficient photocatalytic H<sub>2</sub> evolution has also been recently demonstrated.<sup>[6–8]</sup>

Irradiation of *g*-CN by visible light excites electrons to the conduction band (CB) generating holes in the valence band (VB).<sup>[9]</sup> The electrons in the CB can reduce protons to H<sub>2</sub> in the presence of a suitable cocatalyst whereas holes in the VB can be extracted to a certain extent by sacrificial electron donors during the photocatalytic H<sub>2</sub> evolution reaction (HER). The recombination of holes and electrons, on the other hand, decreases the photocatalytic activity.<sup>[4]</sup> For the efficient photocatalytic H<sub>2</sub> evolution reaction, effective transfer of the electrons from the CB to the catalytic site as well as the transfer of the holes from the VB to the sacrificial agent, are equally important.<sup>[10]</sup> Therefore, the hole extraction from the

[a] Prof. Dr. A. Indra<sup>+</sup>  
Department of Chemistry, Indian Institute of Technology  
Banaras Hindu University  
221005 Varanasi, Uttar Pradesh, (India)  
E-mail: arindam.chy@iitbhu.ac.in

[b] R. Beltrán-Suito,<sup>+</sup> M. Müller, Dr. M. Schwarze, Dr. P. W. Menezes,  
Prof. Dr. M. Driess  
Metalorganics and Inorganic Materials, Department of Chemistry  
Technische Universität Berlin  
Straße des 17 Juni 135, Sekr. C2, 10623 Berlin (Germany)  
E-mail: prashanth.menezes@mailbox.tu-berlin.de  
matthias.driess@tu-berlin.de


[c] Dr. R. P. Sivasankaran, Prof. Dr. A. Brückner  
Leibniz Institute for Catalysis  
University of Rostock  
Albert-Einstein-Str. 29a, 18059 Rostock (Germany)


[d] A. Acharjya, Prof. Dr. A. Thomas  
Functional Materials, Department of Chemistry  
Technische Universität Berlin  
Hardenbergerstraße 40, 10623 Berlin (Germany)

[e] Dr. B. Pradhan, Prof. Dr. J. Hofkens  
Department of Chemistry  
KU Leuven  
Celestijnenlaan 200F, 3001 Heverlee (Belgium)

[f] Prof. Dr. J. Hofkens  
Max Planck Institute for Polymer Research  
Ackermannweg 10, 55128 Mainz (Germany)

[\*] These authors contributed equally to this work.

 Supporting information for this article is available on the WWW under <https://doi.org/10.1002/cssc.202002500>

 © 2020 The Authors. ChemSusChem published by Wiley-VCH GmbH. This is an open access article under the terms of the Creative Commons Attribution Non-Commercial NoDerivs License, which permits use and distribution in any medium, provided the original work is properly cited, the use is non-commercial and no modifications or adaptations are made.

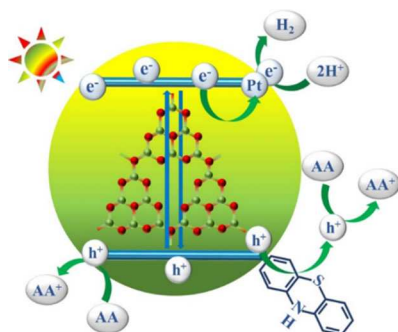
VB by minimizing the recombination of charges is crucial to improve the proton reduction efficiency.

In this regard, a hole acceptor, phenothiazine (PTZ), has been effectively employed to extract the holes from the VB of CdS.<sup>[11]</sup> Similarly, PTZ-modified CdSe quantum dots were shown to improve hole transfer during photocatalytic HER.<sup>[12]</sup> Different derivatives of PTZ were also studied for the photocatalytic HER by combining them with a TiO<sub>2</sub> photocatalyst.<sup>[13]</sup> In addition, PTZ-based molecules were successfully explored as hole-transfer agents to improve the efficiency of solar cells.<sup>[14]</sup> Two main factors directly control the use of PTZ as an ideal hole-transfer agent during the photocatalytic process: (i) one-electron oxidation of PTZ to form the cationic radical (PTZ<sup>•+</sup>) with high stability and (ii) thermodynamically favorable hole transfer from the VB of *g*-CN [1.47 V vs. normal hydrogen electrode (NHE)] to the highest occupied molecular orbital (HOMO) of PTZ (0.9 V vs. NHE).<sup>[15]</sup>

Although Durrant and co-workers reported that the photophysics of *g*-CN materials are similar to that of inorganic semiconductors,<sup>[16]</sup> the role of the hole-transport agents (HTAs) on the photocatalytic properties of *g*-CN or, in a broader context, to photoactive organic polymers remains unexplored. In this work, the role of different HTAs for extracting the holes from the VB of sol-gel-prepared graphitic carbon nitride (*sg*-CN), when irradiated with visible light, is explored (Figure 1). Three different substrates, PTZ, phenazine (PZN), and phenoxazine (POZ), were employed to understand the role of hole acceptors during photocatalytic H<sub>2</sub> evolution with Pt deposited on *sg*-CN (Pt-*sg*-CN) in the presence of ascorbic acid (AA) as the sacrificial electron



**Figure 1.** Hole acceptors employed together with Pt-loaded *sg*-CN in the presence of ascorbic acid as the sacrificial agent during visible-light-driven photocatalytic H<sub>2</sub> evolution.



**Scheme 1.** Schematic representation of the photocatalytic H<sub>2</sub> evolution process employing Pt-*sg*-CN as the photocatalyst, AA as the electron donor, and PTZ as the HTA under visible light irradiation.

donor (Scheme 1 and Tables S1–S5 in the Supporting Information). A remarkable increase in the rate of the H<sub>2</sub> production was observed when PTZ and POZ were used as the hole acceptors. The highest photocatalytic activity was obtained when PTZ was added to a mixture of Pt-*sg*-CN and AA (4.84 times increment in the rate of H<sub>2</sub> production).

Electron paramagnetic resonance (EPR) studies confirmed the effective hole extraction from the VB of *sg*-CN in the presence of PTZ with a decrease in the recombination of the photogenerated charges. Photoluminescence (PL) spectroscopic studies also revealed the improved charge transfer by minimizing electron–hole recombination in the presence of PTZ. Notably, an optimum amount of the acceptor for efficient hole transfer is observed reaching its maximum when 0.25 wt% of PTZ is used. Moreover, Pt-*sg*-CN-PTZ 0.25% continuously produced H<sub>2</sub> for 3 days indicating the long-term durability of the photocatalytic system.

Pt was deposited on *sg*-CN by a microemulsion method following our previously reported procedure (see Experimental in the Supporting Information).<sup>[17]</sup> First of all, three different organic molecules, PTZ, POZ, and PZN, were loaded (0.25 wt%) on Pt-*sg*-CN and characterized by powder X-ray diffraction (PXRD; Figure S1). PXRD analyses showed the peaks at 2 $\theta$  values of approximately 13 and 27° corresponding to the intra-planar heptazine unit distance and the inter-planar stacking arrangement in layered *g*-CN, respectively.<sup>[8]</sup> Solid-state cross-polarization magic angle spinning (CP/MAS) <sup>13</sup>C NMR spectra of the PTZ-loaded Pt-*sg*-CN exhibited peaks at 154 and 162 ppm for CN<sub>3</sub> and C(N)<sub>2</sub>(NH)<sub>x</sub> moieties of the heptazine based system, whereas no extra peak corresponding to PTZ was detected (Figure S2).<sup>[8]</sup> UV/Vis spectra revealed an increment in the visible light absorption after loading of the HTAs on Pt-*sg*-CN (Figure S3) whereas no significant change was detected in the IR spectra (Figure S4). Transmission electron microscopic (TEM) studies displayed 3–4 nm Pt nanoparticles (NPs) supported on sheet-like carbon nitride in PTZ-loaded Pt-*sg*-CN (Figure S5). Energy-dispersive X-ray spectroscopy (EDX) and inductively coupled plasma atomic emission spectroscopy (ICP-AES) further quantified the presence of Pt ( $\approx$  2%, Figure S6 and Table S6). Elemental analyses could not detect any change in the atomic ratio of C/N ( $\approx$  1.46 for *sg*-CN) after the loading of the HTA on *sg*-CN (Table S7).

The oxidation state of Pt in PTZ-Pt-*sg*-CN was analyzed by X-ray photoelectron spectroscopy (XPS) (Figure S7). The Pt 4f<sub>7/2</sub> and 4f<sub>5/2</sub> peaks showed two pairs located at 71.6/74.9 and 72.5/75.5 eV indicating the presence of Pt<sup>0</sup> and Pt<sup>II</sup> species, respectively.<sup>[18]</sup> The C 1s, N 1s, and O 1s XPS spectra of PTZ-Pt-*sg*-CN were matched with previously reported literature and discussed in the Supporting Information (Figures S8–S10).<sup>[8]</sup> EDX mapping showed a homogeneous distribution of the elements C, N, O, and Pt along with S, after the loading of PTZ (Figure S11). The Brunauer–Emmett–Teller (BET) surface area of Pt-*sg*-CN was determined to be 147.8 m<sup>2</sup>g<sup>−1</sup>, and a reduction of the surface area was observed after loading of the HTAs, which points to the

incorporation of PTZ within the pores accompanied by a partial pore blocking (Figure S12, Table S8).

The role of PTZ, POZ, and PZN was investigated as the HTA for the photocatalytic H<sub>2</sub> evolution with Pt-*sg*-CN in the presence of AA as the sacrificial electron donor under sunlight simulation (AM 1.5 G, 300 W). A significant improvement in the photocatalytic HER was observed when PTZ or POZ were employed as the hole carrier along with AA (Figure 2a). However, no such increment in H<sub>2</sub> production was recorded with PZN. The amount of produced H<sub>2</sub> (mmol) with 2% PTZ was 2.74 times higher compared to the reaction carried out without any HTA after 20 h of photocatalytic reaction (Figure 2). The difference is more pronounced (4.84 times) when 0.25% PTZ was used as the HTA in a 20 h experiment (Figure 2a). In the presence of 2 and 0.25% POZ, the increment was 1.76 and 2.30 times higher compared to the reaction with no hole acceptor. As the sacrificial electron donor was the same (AA), the enhancement in the H<sub>2</sub> production confirmed the effective hole transfer from the VB of Pt-*sg*-CN to the HOMO of PTZ or POZ under irradiation with the sunlight simulator.

The photocatalytic HER was further optimized by varying the amount of PTZ to determine the best reaction condition (Figure S13). It was observed that the amount of H<sub>2</sub> production was highly dependent on the amount of PTZ, which attained a maximum at 0.25% and slightly drops to reach a plateau in the presence of an excess amount. This result indicates a limiting amount of hole transfer from the VB of Pt-*sg*-CN to the HOMO of PTZ, and the excess amount of PTZ leads to a saturation point. It is worth to mention here that the photocatalytic H<sub>2</sub> evolution with PTZ-CdS or PTZ-CdSe was studied without loading of any cocatalyst.<sup>[11–12]</sup> As a cocatalyst significantly facilitates the electron transfer from the CB of the photocatalyst to protons, without cocatalyst the overall photocatalytic process is affected. Therefore, we chose to investigate the photocatalytic H<sub>2</sub> evolution with a cocatalyst (Pt)-loaded *sg*-CN and only bare *sg*-CN in the presence of PTZ and AA. Without Pt loading, the amount of produced H<sub>2</sub> with *sg*-CN and AA is negligible, and even the addition of PTZ does not improve the H<sub>2</sub> production (Figure S14).

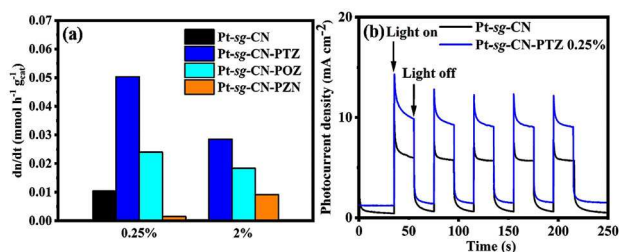


**Figure 2.** (a) Effects of different hole-acceptor agents (PTZ, POZ, and PZN) for the hole acceptance from the VB of Pt-*sg*-CN in the presence of AA as the sacrificial agent during visible-light-driven photocatalytic H<sub>2</sub> evolution. (b) Transient photocurrent measurements for Pt-*sg*-CN and PTZ-Pt-*sg*-CN at a constant potential of approximately 0.5 V vs. Ag/AgCl reference electrode in 0.1 M Na<sub>2</sub>SO<sub>4</sub> under the light on/off condition.

Under the best reaction condition (Pt-*sg*-CN-PTZ 0.25% and AA), the rate of photocatalytic H<sub>2</sub> production was 0.05 mmolH<sub>2</sub>g<sub>cat</sub><sup>-1</sup>h<sup>-1</sup>. This rate is higher than the rates obtained with other graphitic carbon nitride-based catalyst systems when Pt is used as the cocatalyst in the presence of sacrificial agent AA (pH ≈ 3; Table S9).<sup>[19]</sup> Moreover, a continuous H<sub>2</sub> evolution for almost 3 days was recorded with PTZ-Pt-*sg*-CN under sunlight simulation irradiation that showed the long-term durability of the system. Furthermore, we also compared the activity of Pt-*sg*-CN-PTZ 0.25% with respect to the effect of the light source by using 300 W Xe lamp with a 420 nm cut-off filter that indeed displayed significantly enhanced H<sub>2</sub> production (almost 1.5 times) compared to the sunlight simulator and was highly promising compared to the related systems (Figure S15, Table S10). We have carried out electrospray ionization (ESI) MS measurements to confirm that during photocatalysis the adsorbed PTZ on the surface of Pt-*sg*-CN is responsible for the hole transfer and it does not leach out into the solution (Figure S16). ESI-MS of the solution after photocatalysis did not detect any peak of PTZ and showed signals only related to AA, which confirmed our hypothesis.

It is noteworthy that a better photocatalytic activity can be achieved with *sg*-CN or related materials when triethanolamine (TEOA) is used as a sacrificial agent, rather than AA.<sup>[4]</sup> However, the photocatalytic activity studies using PTZ as the HTA cannot be carried out in TEOA, as PTZ is oxidized to phenothiazinone in an aqueous solution at pH > 5 (Figure S17).<sup>[20]</sup> Therefore, we have carried out the photocatalytic hydrogen evolution reactions in AA solution (pH = 2.73) instead of the TEOA solution (1:9 TEOA/H<sub>2</sub>O solution: pH = 7.76).

A negligible amount of photocatalytic H<sub>2</sub> evolution was detected from the control experiments of Pt and AA (without the addition of *sg*-CN). Further, we have carried out the photocatalytic hydrogen evolution with Pt-*sg*-CN-PTZ 0.25% in D<sub>2</sub>O to confirm the source of protons. GC-MS confirmed D<sub>2</sub> as the major product (87%) while a small amount of HD (9%) and H<sub>2</sub> (4%) was detected because of D<sup>+</sup> exchange with AA (Figure S18). This result clearly established water as the source of hydrogen and not the sacrificial agent AA. For a comparison purpose, the apparent quantum efficiency (AQE) with Pt-*sg*-CN-PTZ 0.25% was determined at two different wavelengths. At 415 and 440 nm, the highest AQE was determined to be 0.32 and 0.25%, respectively.

The charge-transfer properties of Pt-*sg*-CN and PTZ-Pt-*sg*-CN were further examined by transient photocurrent measurements and electrochemical impedance spectroscopic (EIS) analyses (Figures 2b and S19). Nyquist plots confirmed a better charge transport in the presence of PTZ compared to only Pt-*sg*-CN under visible light irradiation and even in the dark (Figure S19). Improvement in transient photocurrent with Pt-*sg*-CN was also recorded in the presence of PTZ at a constant potential (at 0.5 V vs. Ag/AgCl, Figure 2b).

The effect of the HTA on charge separation, migration, and recombination was studied in detail by time-resolved photoluminescence (TRPL). Recently, Durrant and co-workers

reported sub-ps time-scale charge separation in *g*-CN, while the long-lived ( $> \mu\text{s}$ ) holes and electrons are unavailable for the next step, to facilitate photocatalytic  $\text{H}_2$  production.<sup>[16]</sup> They further demonstrated that the photoinduced electron accumulation in the CB of carbon nitride accelerates the charge recombination.<sup>[21]</sup> Similarly, Merschjann et al. disclosed that the electron transport in *g*-CN is in the perpendicular direction of the parallel sheets of the 2D material.<sup>[22]</sup>

The emission peak in the PL spectra originates from the separation of photogenerated electrons and holes, and its intensity can reflect the separation efficiency of charge carriers.<sup>[23]</sup> Consequently, a lower intensity indicates a more effective charge separation and trapping in non-emissive states. In the present case, the Pt-*sg*-CN exhibited a strong emission peak at 465 nm corresponding to the bandgap charge separation and the PL emission peak intensity of Pt-*sg*-CN-PTZ 0.25% was found to be lower than that of Pt-*sg*-CN (Figure S20). This suggested that the electron-hole pair separation is higher in Pt-*sg*-CN-PTZ 0.25% resulting in higher  $\text{H}_2$  production compared to Pt-*sg*-CN. In contrast, we previously reported a decrease in the recombination of the charges and improved electron transport when the cocatalyst  $\text{Ni}_2\text{P}$  was combined with *sg*-CN.<sup>[8]</sup>

Photoinduced hole transfer from Pt-*sg*-CN to HTA was also investigated by TRPL spectroscopy (Figure 3a, Table S11). Photoluminescence lifetime measurements showed that the presence of the HTA reduced the exciton lifetime of *sg*-CN and the quenching increased from PZN to POZ to PTZ. It should be mentioned here that not only the hole transfer but also electron transfer and energy transfer from *sg*-CN to the adsorbate can lead to the exciton quenching. In the present study, we did not consider the energy transfer from *sg*-CN to the adsorbate due to a lack of spectral overlap of *sg*-CN emission ( $\lambda_{\text{max}} = 475 \text{ nm}$ ) and PTZ absorption ( $\lambda_{\text{max}} = 265 \text{ nm}$ ) (Figure S21). In addition, we were able to detect the radical cation ( $\text{PTZ}^{\bullet+}$ ) generated by the hole transfer from photoexcited *sg*-CN (Figure S22).  $\text{PTZ}^{\bullet+}$  showed a strong absorption at 324 nm with a shoulder at 380 nm, well separated from the absorption of PTZ at 265 nm.<sup>[24]</sup> The above results

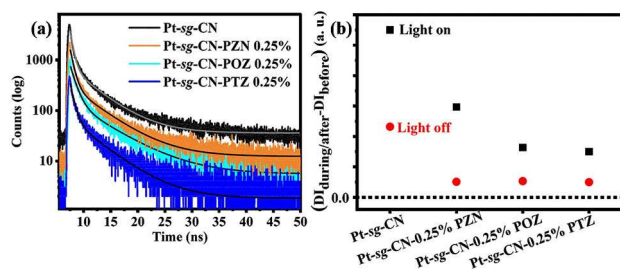


**Figure 3.** (a) Time-resolved trapped-state photoluminescence decay of Pt-*sg*-CN showing decreasing electron-hole recombination in the presence of different hole acceptors. The rate of electron-hole recombination follows the order: Pt-*sg*-CN  $>$  PZN-Pt-*sg*-CN  $>$  POZ-Pt-*sg*-CN  $>$  PTZ-Pt-*sg*-CN. (b) Double integral of the EPR CB electron signal intensity (initial background signal in the dark was subtracted) during visible light irradiation (black squares) and after light switched-off (red dots).

clearly demonstrate that the HTA promotes the dissociation of the photogenerated electron-hole pairs to free charge carriers in excited *sg*-CN.

The process of transferring holes from the photocatalyst to water molecules is more complicated than the transfer of electrons to protons.<sup>[25–26]</sup> The current understanding of the hole-transfer process has been mostly deduced from the photoluminescence quenching of the exciton in the presence of hole acceptor.<sup>[27]</sup> Previously, Kamat and co-workers were able to detect the adsorbate cation formed by the hole transfer from CdSe quantum dots to *p*-phenylenediamine.<sup>[28]</sup> Similarly, the transfer of holes from CdS to PTZ has been described by photoluminescence spectroscopy.<sup>[10]</sup>

Further, in situ EPR studies were carried out to understand the charge recombination and transport properties. Pure *sg*-CN, even in the dark condition, exhibits a narrow isotropic singlet with Lorentzian line shape at a *g*-value of 2.0046, which results from unpaired electrons trapped at  $\text{sp}^2$ -carbon atoms in a typical heptazine unit (Figure S23).<sup>[4]</sup> The EPR signal intensity increased under visible light irradiation due to enhanced excitation and trapping of electrons in the CB and decreased again after light switch-off due to the recombination of photoexcited electrons with holes (Figure S24). This intensity decreases in the following order: Pt-*sg*-CN  $>$  Pt-*sg*-CN-PZN  $>$  Pt-*sg*-CN-POZ  $>$  Pt-*sg*-CN-PTZ (Figure 3b, black symbols), due to the transfer of excited electrons from the CB of *sg*-CN to Pt, where they cannot be detected by EPR. This means, the lower the EPR signal intensity under irradiation, the more effective is electron transfer to the Pt nanoparticles. Comparison of Figure 3b and Figure 2a reveals that the EPR intensity under visible light irradiation is the lowest, that is, electron transfer to Pt is the highest for the most active catalyst Pt-*sg*-CN-PTZ. This is easy to understand, considering that proton reduction takes place on the Pt cocatalyst and a high concentration of electrons might speed up  $\text{H}_2$  formation.

Interestingly, the EPR signals of the catalysts containing HTAs are smaller and broader compared to the signal of pristine Pt-*sg*-CN (Figure S24). This suggests that some transfer of trapped electrons from *sg*-CN to the HTA may occur already in the dark. In principle, this should give rise to radical formation. In Figure S24, a hyperfine structure typical for such kinds of radicals is not resolved, yet it could contribute to the line width, which is highest for the most active Pt-*sg*-CN-PTZ. The significantly stronger dark signal of pristine Pt-*sg*-CN may be due to the fact that an HTA, which could take up a part of the trapped electrons, is missing.

In conclusion, we demonstrated here the effect of hole acceptor molecules to transfer the photogenerated holes from the VB of Pt-*sg*-CN to the sacrificial electron acceptor. EPR and PL studies have shown that the transport of the photogenerated holes becomes faster in the presence of the molecules PTZ and POZ resulting in improved electron-hole separation compared to PZN. In the case of PTZ, the most effective hole transport has been observed with a 4.84 times increase in the rate of photocatalytic HER. Moreover, the PTZ-Pt-*sg*-CN can produce  $\text{H}_2$  for 3 days to exhibit long-term

stability. It is observed that the formation of the radical cation (PTZ<sup>•+</sup>) by one-electron oxidation is the key factor for the facile hole transfer. Further, the photogenerated PTZ<sup>•+</sup> can be utilized as the super-photooxidants to carry out photocatalytic organic reactions. Besides, this study will open a new avenue to develop hole transfer agents, which are stable in alkaline medium (especially in TEOA). This will be highly important to further improve the photocatalytic activity of Pt-*sg*-CN combining HTA and using TEOA as the sacrificial electron donor.

## Experimental Section

### Chemicals

The chemicals were purchased from Sigma Aldrich or Alfa-Aesar and used without further purification.

### Instruments

Powder XRD was recorded in Bruker AXS D8 advanced diffractometer equipped with a position-sensitive detector (PSD) and curved germanium (111) primary monochromator and the radiation used was CuK $\alpha$  ( $\lambda = 1.5418 \text{ \AA}$ ).

The solid-state CP/MAS <sup>13</sup>C{1H} NMR spectra were recorded in a Bruker Advance 400 spectrometer. UV/Vis spectroscopic measurements were performed in Lambda 35 UV/Vis spectrometer from Perkin Elmer (USA). IR spectroscopic studies were performed in BIORAD FTS 6000 Fourier-transform (FT) IR spectrometer under attenuated total reflection (ATR) conditions.

XPS studies were performed in a Kratos Axis Ultra X-ray photoelectron spectrometer (Kratos Analytical Ltd., Manchester, UK) with an AlK $\alpha$  monochromatic radiation source (1486.7 eV) and 90° take-off angle maintaining at  $2 \times 10^{-9}$  Torr pressure in the analyzing chamber. The high-resolution XPS spectra were recorded with a pass energy of 20 eV and a step with 0.1 eV. The binding energies were calibrated with respect to the C 1s peak energy position at 285.0 eV. Data analyses were performed employing Casa XPS (Casa Software Ltd.) and Vision data processing program (Kratos Analytical Ltd.).

SEM was carried out on an LEO DSM 982 microscope integrated with an EDX spectrometer (EDAX, Apollo XPP). Data handling and analyses were achieved with the software package EDAX. Most abundant elements were selected from the EDX spectra. TEM was accomplished on an FEI Tecnai G2 20 S-TWIN transmission electron microscope (FEI Company, Eindhoven, Netherlands) equipped with a LaB<sub>6</sub> source at 200 kV acceleration voltage. EDX analyses were achieved with an EDAX r-TEM SUTW detector (Si (Li) detector) and the images were recorded with a GATAN MS794 P CCD camera. 5 independent EDX measurements were done to determine the C:N ratio and Pt content on Pt-*sg*-CN. The SEM and TEM experiments were conducted at the Zentrum für Elektronenmikroskopie (ZELMI) of the TU Berlin.

The elemental (CHN) analyses were performed on a Thermo Flash EA 1112 Organic Elemental Analyzer by dynamic flash combustion at 1020 °C. BET surface areas were measured with a micromeritics Nova 4200e (Quantachrome Instruments) surface-area analyzer using nitrogen adsorption at 77 K. ICP-AES was carried out in a Thermo Jarrell Ash Trace Scan analyzer. The samples were digested in aqua regia HCl/HNO<sub>3</sub> 3:1 v/v (nitric acid, SUPRA-Qualität

ROTIPURAN® Supra 69% and hydrochloric acid, SUPRA-Qualität ROTIPURAN® Supra 30%) and the average of three reproducible independent experiments is reported. The digestion volume (2.5 mL) was diluted with Milli-Q water up to 15 mL. Calibration curves were prepared for Pt with concentrations between 1 mg L<sup>-1</sup> and 100 mg L<sup>-1</sup> from standard solutions (1000 mg L<sup>-1</sup>, Single-Element ICP-Standard Solution ROTI®STAR).

High-resolution ESI-MS was measured on a Thermo Scientific LTQ orbitrap XL. The analyzed solution was taken from the supernatant after 20 h of photocatalysis and injected directly into the spectrometer.

### Synthesis of Pt-*sg*-CN

Carbon nitride, *sg*-CN was synthesized according to the literature-reported procedure.<sup>[3]</sup> Pt loading on *sg*-CN was carried out by employing a microemulsion method.<sup>[17]</sup> The metal precursor (H<sub>2</sub>PtCl<sub>6</sub>, 8 wt% solution) was reduced by using ascorbic acid (50:1 molar ratio). All solutions were freshly prepared before use. First, metal precursor solution A was prepared by mixing 45 g cyclohexane, 20 g 1-pentanol, 20 g TX-100, and 0.525 mL H<sub>2</sub>PtCl<sub>6</sub> in 15 mL water and stirred at 720 rpm at 298 K for 10 min. Reducing solution B was prepared by mixing 45 g cyclohexane, 20 g 1-pentanol, 20 g TX-100, and 0.8815 g ascorbic acid in 15 mL water. Reducing solution B was added to the platinum precursor solution and stirred for 1 h at 25 °C. Next, the photocatalyst (1 g *sg*-CN) was added into the mixture and stirred for 10 min at 320 rpm. The temperature was increased to 45 °C and stirred for 2 h. The mixture was cooled down to room temperature, and the solid was separated by centrifugation at 7500 rpm for 10 min. The solid catalyst was washed with acetone (3 times) and dried overnight at 80 °C under reduced pressure (80 mbar).

### Incorporation of hole-transfer agents

Initially, concentrated solutions (5 mg mL<sup>-1</sup>) of PTZ, PZN, and POZ were prepared by dissolving 25 mg of the hole transfer agent in 5 mL EtOH. The concentrated solution was diluted to prepare the solutions of desired concentration (0.10, 0.25, 0.50, 1, 2, and 10% of loading in Pt-*sg*-CN). 60 mg of Pt-*sg*-CN was dispersed in 5 mL solution of the HTA in EtOH (Tables S1–S3) to give materials with different amounts of the incorporated HTA. The mixture was sonicated for 2 h, followed by stirring for 1 h at 500 rpm. The solid catalyst was separated from the solution by centrifugation (5000 rpm, 10 min). The solid was washed with acetone and dried overnight at room temperature. The final concentration of the HTA in the solution was determined by UV/Vis spectroscopy. The amount of incorporated HTA was calculated from the difference in the initial concentration of the solution and after the loading on Pt-*sg*-CN.

### Photocatalytic hydrogen evolution

Photocatalytic hydrogen evolution reactions were carried out in a 60 mL Teflon reactor fitted with a quartz glass side window. The temperature of the reaction mixture was maintained at  $30 \pm 1$  °C by using a temperature controller. 25 mg catalyst, 1.33 g AA, and 38 mL water were kept inside the photoreactor, degassed by purging Ar for 30 min and irradiated with a sunlight simulator (LOT LS0308). This consists of a 300 W Xe lamp with an AM 1.5G filter, which creates a spectrum similar to sunlight. The distance between the lamp and the reactor is always 10 cm. The long-term experiment was also done using the 420 nm cut-off filter. The increase of pressure was measured for 20 h (70 h for the long-term experi-

ments). The obtained gas mixture from the headspace was injected into GC to determine the vol% of H<sub>2</sub>. The amount of evolved H<sub>2</sub> gas (mmol, conversion factor 24.87 L mol<sup>-1</sup> at 30 °C) was calculated from the obtained % of H<sub>2</sub>, and the pressure increase during the measurements. The irradiation area of the light was 19.63 cm<sup>2</sup>.

### Photoelectrochemical measurements

Inks of different catalysts were prepared by dispersing 5 mg of catalysts (Pt-*sg*-CN or Pt-*sg*-CN-PTZ 0.25 %) using 0.05 % Nafion solution in ethanol as the binder. 500 μL of each solution was drop cast on indium-doped tin oxide (ITO) to cover a geometric surface area of 1 cm<sup>2</sup>. Photoelectrochemical measurements were carried out in 0.1 M Na<sub>2</sub>SO<sub>4</sub> solution with a three-electrode set up having a catalyst on ITO as the working electrode, Pt wire as the counter electrode and Ag/AgCl as the reference electrode. 0.5 V constant potential vs Ag/AgCl was applied with the light on-off after a certain time interval to record the photo and dark current. Visible light irradiation of 400–700 nm was applied for photocurrent measurements and EIS analyses.

### EPR spectroscopy studies

In situ EPR measurements in X-band (microwave frequency ≈ 9.8 GHz) were performed at 300 K by a Bruker EMX CW-micro spectrometer equipped with an ER 4119HS-WI high-sensitivity optical resonator with a grid in the front side. The samples were illuminated by a 300 W Xe lamp with a 420 nm cut-off filter (LOT Oriol). All the samples were measured under the same conditions (microwave power: 6.99 mW, receiver gain: 1 × 10<sup>4</sup>, modulation frequency: 100 kHz, modulation amplitude: 3 G, sweep time: 122.8 s). *g* values have been calculated from the resonance field *B*<sub>0</sub> and the resonance frequency *ν* using the resonance condition  $h\nu = g\beta B_0$ . The calibration of the *g* values was performed using DPPH (2,2-diphenyl-1-picrylhydrazyl) (*g* = 2.0036 ± 0.00004).

### Photoluminescence

PL spectra were obtained by a Cary Eclipse Fluorescence spectrophotometer (Agilent Technologies Inc., Mulgrave, Australia) with an excitation wavelength of 360 nm. PL emission spectra can be measured in low, medium, and high detector voltage (photomultiplier tube, PMT is the detector). The pulse energy of the pump beam was about 460 nJ per pulse at the sample and the excitation spot had a 1/e<sup>2</sup> diameter of 680 μm. The TRPL spectra were recorded by a streak camera system (Streakscope C10627, Hamamatsu). The recorded data sets for three-time windows (5, 200, and 5000 ns) were combined into one time-resolved spectrum.

### Time-resolved photoluminescence

The TRPL lifetimes were probed by using Leica TCS SP8 X confocal fluorescence microscope on a cover slide by drop-casting the sample from water dispersion. A 405 nm diode laser with 20 MHz repetition rate has been used to measure the lifetime following photoexcitation in fluorescence lifetime imaging (FLIM) mode. The inbuilt software has been used to fit the lifetime of biexponential decays.

### Photoexcitation of PTZ and generation of radical cation PTZ<sup>•+</sup>

A mixture of 2 mg PTZ and 5 mg AA in 10 mL of water was sonicated for 30 min to prepare a suspension, and the UV/Vis absorption spectrum was recorded. 5 mg of Pt-*sg*-CN were added to the mixture and sonicated for 10 min with visible light irradiation (400–700 nm, LUMATEC light source, SUPERLITE 400). The UV/Vis absorption spectrum was measured immediately to detect the generated PTZ<sup>•+</sup>.

### Acknowledgements

*A.I. acknowledges the financial support from CSIR, India. R.B.S. is grateful for the support by the Einstein Foundation Berlin (ESB) – Einstein Center of Catalysis (EC<sup>2</sup>). B.P. acknowledges a postdoctoral fellowship from the Research Foundation-Flanders (FWO Grant No. 1275521 N). J.H. acknowledges financial support from the Research Foundation-Flanders (FWO, Grant No. G983.19 N, G0 A5817 N, and G0H6316 N) and the Flemish government through long-term structural funding Methusalem (CASAS2, Meth/15/04). Funded by the Deutsche Forschungsgemeinschaft (DFG, German Research Foundation) under Germany's Excellence Strategy–EXC 2008/1–390540038–UniSysCat. Open access funding enabled and organized by Projekt DEAL.*

### Conflict of Interest

The authors declare no conflict of interest.

**Keywords:** charge separation · graphitic carbon nitride · hole transfer · hydrogen evolution · photocatalyst

- [1] H. B. Gray, *Nat. Chem.* **2009**, *1*, 7.
- [2] a) S. Chen, T. Takata, K. Domen, *Nat. Rev. Mater.* **2017**, *2*, 17050; b) A. Indra, P. W. Menezes, M. Schwarze, M. Driess, *New J. Chem.* **2014**, *38*, 1942–1945; c) P. W. Menezes, A. Indra, M. Schwarze, F. Schuster, M. Driess, *ChemPlusChem* **2016**, *81*, 1068–1074.
- [3] K. Kailasam, J. D. Epping, A. Thomas, S. Losse, H. Junge, *Energy Environ. Sci.* **2011**, *4*, 4668–4674.
- [4] W. J. Ong, L. L. Tan, Y. H. Ng, S. T. Yong, S. P. Chai, *Chem. Rev.* **2016**, *116*, 7159–7329.
- [5] L. Lin, Z. Yu, X. Wang, *Angew. Chem. Int. Ed.* **2019**, *58*, 6164–6175; *Angew. Chem.* **2019**, *131*, 6225–6236.
- [6] a) L. Kong, Y. Dong, P. Jiang, G. Wang, H. Zhang, N. Zhao, *J. Mater. Chem. A* **2016**, *4*, 9998–10007; b) J. Hong, Y. Wang, Y. Wang, W. Zhang, R. Xu, *ChemSusChem* **2013**, *6*, 2263–2268.
- [7] A. Indra, P. W. Menezes, K. Kailasam, D. Hollmann, M. Schröder, A. Thomas, A. Brueckner, M. Driess, *Chem. Commun.* **2016**, *52*, 104–107.
- [8] A. Indra, A. Achariya, P. W. Menezes, C. Merschjann, D. Hollmann, M. Schwarze, M. Aktas, A. Friedrich, S. Lochbrunner, A. Thomas, M. Driess, *Angew. Chem. Int. Ed.* **2017**, *56*, 1653–1657; *Angew. Chem.* **2017**, *129*, 1675–1679.
- [9] J. Zhang, Y. Chen, X. Wang, *Energy Environ. Sci.* **2015**, *8*, 3092–3108.
- [10] L. Kong, Y. Ji, Z. Dang, J. Yan, P. Li, Y. Li, S. Liu, *Adv. Funct. Mater.* **2018**, *28*, 1800668.
- [11] a) S. Lian, D. J. Weinberg, R. D. Harris, M. S. Kodaimati, E. A. Weiss, *ACS Nano* **2016**, *10*, 6372–6382; b) K. Wu, Y. Du, H. Tang, Z. Chen, T. Lian, *J. Am. Chem. Soc.* **2015**, *137*, 10224–10230.

- [12] B. Li, M. Wen, Y. J. Gao, H. L. Wu, M. Y. Huang, Z. J. Li, B. Chen, C. H. Tung, L. Z. Wu, *Adv. Sci.* **2016**, *3*, 1500282.
- [13] J. Lee, J. Kwak, K. C. Ko, J. H. Park, J. H. Ko, N. Park, E. Kim, D. H. Ryu, T. K. Ahn, J. Y. Lee, S. U. Son, *Chem. Commun.* **2012**, *48*, 11431–11433.
- [14] Y. Rout, R. Misra, R. Singhal, S. Biswas, G. D. Sharma, *Phys. Chem. Chem. Phys.* **2018**, *20*, 6321–6329.
- [15] D. Cummins, G. Boschloo, M. Ryan, D. Corr, S. N. Rao, D. Fitzmaurice, *J. Phys. Chem. B* **2000**, *104*, 11449–11459.
- [16] R. Godin, Y. Wang, M. A. Zwijnenburg, J. Tang, J. R. Durrant, *J. Am. Chem. Soc.* **2017**, *139*, 5216–5224.
- [17] R. Y. Parapat, M. Wijaya, M. Schwarze, S. Selve, M. Willinger, R. Schomäcker, *Nanoscale* **2013**, *5*, 796–805.
- [18] a) E. I. Vovk, A. V. Kalinkin, M. Y. Smirnov, I. O. Klembovskii, V. I. Bukhtiyarov, *J. Phys. Chem. C* **2017**, *121*, 17297–17304; b) F. Şen, G. Gökağac, *J. Phys. Chem. C* **2007**, *111*, 5715–5720.
- [19] a) J. Albero, E. M. Barea, J. Xu, I. Mora-Seró, H. Garcia, M. Shalom, *Adv. Mater. Interfaces* **2017**, *4*, 1600265; b) H. Li, Y. Xia, T. Hu, Q. Deng, N. Du, W. Hou, *J. Mater. Chem. A* **2018**, *6*, 6238–6243.
- [20] a) D. J. Cavanaugh, *J. Am. Chem. Soc.* **1959**, *81*, 2507–2515; b) P. Hanson, R. O. C. Norman, *J. C. S. Perkin II* **1973**, 264–271.
- [21] W. Yang, R. Godin, H. Kasap, B. Moss, Y. Dong, S. A. J. Hillman, L. Steier, E. Reisner, J. R. Durrant, *J. Am. Chem. Soc.* **2019**, *141*, 11219–11229.
- [22] C. Merschjann, S. Tschierlei, T. Tyborski, K. Kailasam, S. Orthmann, D. Hollmann, T. Schedel-Niedrig, A. Thomas, S. Lochbrunner, *Adv. Mater.* **2015**, *27*, 7993–7999.
- [23] M. Z. Rahman, C. B. Mullins, *Acc. Chem. Res.* **2019**, *52*, 248–257.
- [24] T. Rodrigues, C. G. dos Santos, A. Ripoati, L. R. S. Barbosa, P. D. Mascio, R. Itri, M. S. Baptista, O. R. Nascimento, I. L. Nantes, *J. Phys. Chem. B* **2006**, *110*, 12257–12265.
- [25] C. Merschjann, T. Tyborski, S. Orthmann, F. Yang, K. Schwarzburg, M. Lublow, M. C. Lux-Steiner, T. Schedel-Niedrig, *Phys. Rev. B* **2013**, *87*, 205204–205208.
- [26] W.-J. Ong, L.-L. Tan, Y. H. Ng, S.-T. Yong, S.-P. Chai, *Chem. Rev.* **2016**, *116*, 7159–7329.
- [27] C. Landes, C. Burda, M. Braun, M. A. El-Sayed, *J. Phys. Chem. B* **2001**, *105*, 2981–2986.
- [28] S. N. Sharma, Z. S. Pillai, P. V. Kamat, *J. Phys. Chem. B* **2003**, *107*, 10088–10093.

---

Manuscript received: October 26, 2020  
Revised manuscript received: November 19, 2020  
Accepted manuscript online: November 19, 2020  
Version of record online: November 27, 2020